Electron paramagnetic resonance of Gd^{3+} in C_S symmetry and crystallographic study of rare-earth ultraphosphates. Case of Gd^{3+}, Eu^{3+}, and Gd_xEu_{1-x} ultraphosphates

R. Parrot, C. Barthou, and B. Canny
Laboratoire de Luminescence II-Université de Paris VI, Tour 13, 4, place Jussieu, 75230 Paris Cedex 05, France

B. Blanzat
Laboratoire de Recherche sur les Terres Rares, Centre National de la Recherche Scientifique, Groupe des Laboratoires de Bellevue, 1, place Aristide Briand, 92190 Meudon, France

G. Collin
Laboratoire de Chimie Structurale, Faculté des Sciences Pharmaceutiques et Biologiques, 4, av. de l'Observatoire, 75270 Paris Cedex 06, France

(Received 12 February 1974)

The electron paramagnetic resonance of GdP_5O_{14} and of mixed Gd_xEu_{1-x} ultraphosphates has been studied. The Gd ultraphosphate shows a strong anisotropic structure, but the observed linewidths of the order of several-hundred gauss forbid a detailed analysis of the local symmetry of gadolinium. However, mixed samples containing predominantly Eu^{3+} and 5×10^{-2} at.% of gadolinium show a number of relatively narrow lines (linewidths: 5–10 G). The angular variations of the allowed and forbidden absorption lines have been fitted to the spin Hamiltonian corresponding to C_S symmetry. Eight different centers have been found, four of them being related to the others by two reflexion planes. A refinement of the crystal structure of europium ultraphosphate EuP_5O_{14} (monoclinic space group $P2_{1/b} - C_{2h}^5$) has been carried out by application of the least-squares method of calculation to single-crystal x-ray data ($R = 0.040$). The cell parameters are $a = 8.744$, $b = 12.949$ and $c = 8.925$ Å, $\gamma = 90.46°$, $Z = 4$. Crystal-structure studies show that the structure consists of PO_4 tetrahedra sharing tops in zig-zag chains running parallel to the b axis and PO_4 tetrahedra loops connecting the chains. The oxygen atoms around the Eu atom form an eight-coordinate polyhedron. The correlations between the crystallographic structure and the EPR results for rare-earth ultraphosphates are discussed in detail.

I. INTRODUCTION

Among all the ions which exhibit an EPR spectrum, the d^5 and f^7 ions are particularly interesting when we are concerned by the local symmetry of the environment of the ion. In fact, all sublevels of the S states are generally observed in low magnetic fields for two reasons: (a) The zero-field splitting is zero to the first order, and (b) only high-order effects permit lifting the degeneracy of the fundamental states ^6S or ^8S.[1] Therefore, a detailed study of the angular variations of the absorption lines permits us in principle to recognize the point symmetry around the magnetic ion.

Numerous experiments were performed on Gd^{3+} in various relatively simple lattices. For example, Abraham *et al.*[2,3] and Bacquet *et al.*[4] studied this ion in cubic symmetry; Rosenthal *et al.*[5,6] and Danner *et al.*[7] studied Gd^{3+} in a zircon structure (D_{2d} point symmetry); Hutchison *et al.*[8] and Bleaney *et al.*[9,10] considered Gd^{3+} in a presumed C_{3h} symmetry.

The present study of rare-earth ultraphosphates (REUP) by EPR method was thus primarily motivated to acquire accurate information regarding the environment of the rare-earth ion. (In particular, optical-absorption experiments on EuP_5O_{14}[11] failed to give the correct point symmetry for Eu^{3+} ions. These optical experiments suggested that the site symmetry for Eu^{3+} was C_{2v}).

Our experiments were performed concomittently with a crystallographic study of EuP_5O_{14} and GdP_5O_{14} because the crystal structures found by different authors for single-crystal rare-earth ultraphosphates were not in agreement with each other.

In 1969, Jaulmes[12] concluded an orthorhombic lattice for LaP_5O_{14} (space group P_{nc2} or P_{ncm}).

In 1970, Bagieu-Beucher *et al.*[13] studied the series from lanthanum to lutetium and indicated that these compounds crystallize with three different structure types. The first type from lanthanum to terbium (La, Ce, Pr, Nd, Sm, Eu, Gd, and Tb) was found to be monoclinic with the space group $P_{21/a}$. The second type (Tb, Dy, Ho, Er, Tm, Yb, Lu, and Y) was monoclinic as well with the space group C_c or $C_{2/c}$. The third group (Dy, Ho, Er, and Y) crystallized with an orthorhombic cell and space group $P_{C\,21/m}$ or $P_{C\,mn}$.

Danielmeyer and Weber[14] studied NdP_5O_{14} as a promising candidate for an efficient Nd laser, and contrary to Bagieu-Beucher[13] who typed it as monoclinic, they found that NdP_5O_{14} crystallizes in the orthorhombic system with a space group P_{mna}.

In 1972, Duc Tranqui *et al.*[15] determined the first structure with interatomic distances and angles of

a rare-earth ultraphosphate (HoP_5O_{14}). They found an orthorhombic unit cell with a space group P_{nma}.

In 1974, Hong and Pierce[16] reported the structure of YbP_5O_{14} (space group $C_{2/c}$) and Albrand *et al.*[17] found a pseudo-orthorhombic structure (space group $P_{21/c}$) for NdP_5O_{14}. This last result being in agreement with the conclusions reached by Bagieu-Beucher but in disagreement with those of Danielmeyer and Weber, Albrand *et al.* suggested two hypotheses to explain the contradictory structures obtained for NdP_5O_{14}: (i) Either the frequent twinnings observed in the (001) plane could lead to erroneous space-group assignments, (ii) or NdP_5O_{14} could be grown with different structures, the structure depending on the growing temperature.

The above results led us to be very cautious in our study and consequently to determine the structure of the crystals used in our experiments.

Due to the width of the EPR absorption lines, no definite result was obtained with GdUP crystals, only a strong anisotropy of the spectra appearing. Samples of mixed (Gd, Eu) UP were then grown, the determination of the site symmetry and of the parameters of the spin Hamiltonian were performed with these crystals.

The sample preparation and the general features of the EPR spectra and the angular variations are given for GdP_5O_{14} and (Gd, Eu) P_5O_{14} in Sec. II. In Sec. III, the parameters of the spin Hamiltonian are determined first from perturbation formulas using a least-mean-squares-fit method, and then compared to those obtained by a direct diagonalization of the spin Hamiltonian. We show that the angular variations are in accord with crystallographic results giving a site symmetry C_S. The different sites observed in EPR experiments are then analyzed in Sec. IV by taking into account the results given by x-ray measurements. It is shown that Gd^{3+} ions are related four by four by mirror planes.

II. EXPERIMENTS

A. Crystal growing

For the GdP_5O_{14} crystal growing, we used a Gd_2O_3 oxide purified by an ion-exchange technique (purity: 99.999%). These crystals were grown as described by Blanzat *et al.*[11] The single crystals EuP_5O_{14} doped with trivalent gadolinium were prepared in the following manner: The oxydes Eu_2O_3 and Gd_2O_3 in the ratio of 500 ppm of Gd_2O_3, were dissolved, coprecipitated as oxalates, dried, ignited, and then heated for 2 h in air at 1400 °C in "morganite" boats. The purity of Eu_2O_3 oxydes was 99.999%.

The gadolinium used for the crystal growing contained both odd isotopes (^{155}Gd, natural abundance 14.76%[18]; ^{157}Gd, natural abundance 15.71%[18]), and even isotopes with zero nuclear spin.

B. Samples and experimental procedure

A careful examination of the crystals with a microscope revealed that the crystals were well shaped and multifaceted. The dimensions of the crystals used in EPR experiments are of the order of $0.5\times0.5\times0.5$ mm^3, their external shape is given in Fig. 1 (a).

Anticipating the crystallographic results (Sec. IV A), there are four molecules per unit cell in rare-earth ultraphosphates, the number of rare-earth ions being about 4×10^{21} ions per cm^3. Therefore, 2.5×10^{14} Gd^{3+} ions are present in mixed (Gd, Eu) UP samples and 5×10^{17} Gd^{3+} ions are in Gd UP.

The experiments were performed at room temperature with a Varian 4502 spectrometer operating in the *Ka* band (35.55 GHz) and in the *X* band (9.2 GHz). The samples were carefully fixed in the cavity which was itself well oriented in the magnetic field. The influence of a slight disorientation of the horizontal plane in which the magnetic field was rotated was studied for each angular variation. Each angular variation was made at least three times with different samples in order to verify the correctness of the position of the sample and of the cavity with respect to the magnetic field. The angular variations were performed with $\vec{H}$ rotating in the well-defined growing planes parallel or perpendicular to the $\vec{z}$ axis defined in Fig. 1.

C. Case of GdP_5O_{14}

A spectrum corresponding to $\vec{H}$ in the $(\vec{x},\vec{y})$ plane is given in Fig. 2(a) extending over 11.5 KG. Five lines appear on the extremities of the spectrum and the central part shows a very broad absorption line with some structure. The linewidths are greater than or equal to 900 G. The spectrum in Fig. 2(a) can be compared to that represented in Fig. 2(b) which was obtained with a mixed (Gd, Eu) UP crystal giving well-defined lines. The angular variations for GdUP are significant for the transitions $\pm\frac{7}{2}\leftrightarrow\pm\frac{5}{2}$ and $\pm\frac{5}{2}\leftrightarrow\pm\frac{3}{2}$ for $\vec{H}$ rotating in the $(\vec{x},\vec{y})$ plane and for $-30°<\theta<+30°$ and $60°<\theta<120°$. That is, they are identical to those obtained with (Gd, Eu) UP ($\theta=0°$ corresponds to $\vec{H}\parallel\vec{x}$). Other angular variations like the ones defined in Sec. III were performed and gave well-defined absorption lines for very small angular variations so that a definite analysis of the symmetry was impossible in this case.

D. Case of (Gd_xEu_{1-x}) UP

Mixed ultraphosphate was prepared in order to get much more resolved spectra. The concentration corresponded to $x=5\times10^{-4}$. A typical spectrum obtained at room temperature is given in Fig. 2(b); all observed lines will be attributed in Sec.

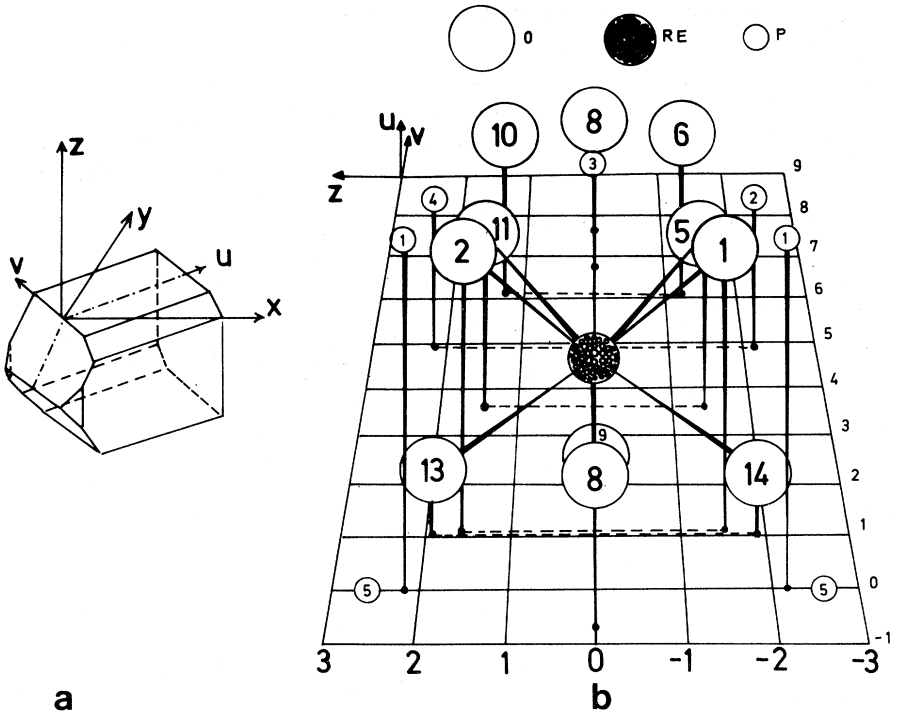

FIG. 1. (a) Typical shape of the rare-earth ultraphosphate crystals used in the experiments; (b) structure of one site for Eu^{3+} showing the pseudo mirror plane associated to the point symmetry C_S and the two pseudo mirror planes $(\vec{u},\vec{z})$, $(\vec{v},\vec{z})$ relating the environment of different Eu^{3+} ions. This structure was deduced from x-ray analysis of the samples. Slight distortions of this structure when Gd^{3+} ions are introduced as impurity in EuUP are described in Sec. IV B.

III B to the allowed transitions $\Delta M_S = 1$ of Gd^{3+}. Of course no line due to Eu^{3+} is expected to be observed at this temperature. The linewidths vary between 5 and 10 G during the angular variations. A splitting of the lines is observed for almost all orientations.

Figure 3 represents the angular variation for $\vec{H}$ rotating in the $(\vec{x},\vec{y})$ plane. The 14 lines observed when $\theta = 0°$ $(\vec{H} \parallel \vec{x})$ correspond to two different sites for Gd^{3+}. For the other orientations, a splitting of each line into at the most four lines is observed, the separation between the outer lines is at the most 80 G (the scale chosen in Fig. 3 does not permit a representation of this splitting).

We must note that the angular variation for the two groups of absorption lines are exactly symmetrical with respect to the axis $\theta = 45°$ and that the angular variation of one group cannot be deduced from the angular variation of the other group simply by a rotation of 90°. In particular, no symmetry axis exists in the angular variations for one group with respect to axes $\theta = 0°$ or 90°. Since this lack of symmetry axis is incompatible with the hypothesis that Gd^{3+} is in a C_{2v} symmetry site, it was important to avoid any misorientation of the samples. Therefore, this angular variation was checked for three different samples.

It must be noted that the intensities of the lines varied considerably during the angular variation and particularly the lines M_S: $+\frac{7}{2} \leftrightarrow +\frac{5}{2}$ and M_S: $-\frac{5}{2} \leftrightarrow -\frac{7}{2}$. The indexation of the lines corresponding to a transition $M_S \rightarrow M_S - 1$ is arbitrary in the sense that the sign for M_S was not defined from experiments at lower temperatures (the indexation was determined from the theoretical results given

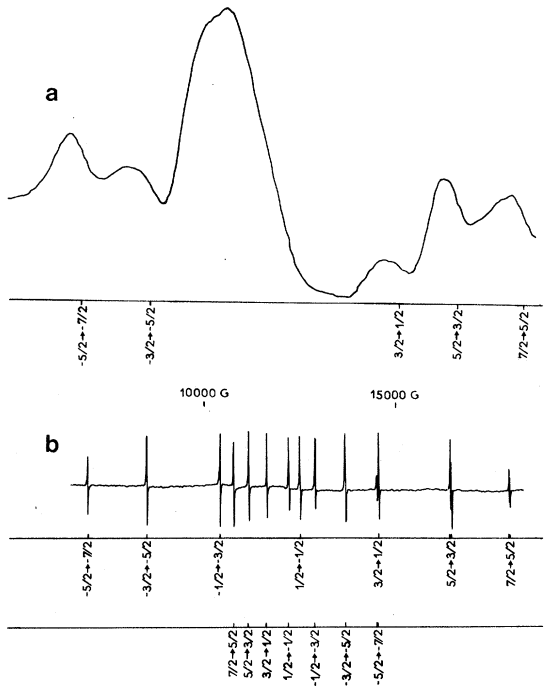

FIG. 2. (a) EPR spectrum obtained with GdUP, $\vec{H}$ is in the $(\vec{x},\vec{y})$ plane at $-2°$ from the x direction; (b) EPR spectrum obtained with (Gd, Eu) UP in the same conditions as for (a).

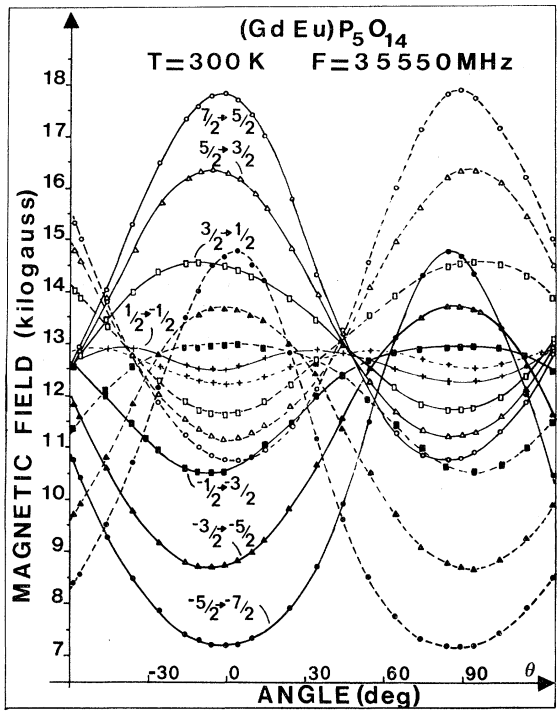

FIG. 3. Angular variations of the authorized absorption lines for Gd^{3+} in (Gd, Eu)UP. $\vec{H}$ is rotated in the $(\vec{x}, \vec{y})$ plane, $\theta = 0°$ corresponds to $\vec{H} \| \vec{x}$.

in Sec. III). The angular variation for $30° \leq \theta \leq 60°$ was carefully performed in order to recognize the lines during the crossings.

Figure 4 gives the angular variation for $\vec{H}$ rotated in the plane $(\vec{v}, \vec{z})$. In this case, the accurate orientation of the samples was performed by comparing the spectra obtained for $\vec{H} \| \vec{v}$ in Figs. 3 and 4; a slight misorientation of the samples gives very different spectra for the absorption lines appearing at higher magnetic field. The angular variation is given for four different groups of absorption lines in Fig. 4. Each group shows two absorption lines separated at the most by 50 G while the overall separation between the groups can attain 1500 G, as it can be seen in Fig. 4 for the transition M_S: $+\frac{7}{2} \rightarrow +\frac{5}{2}$.

Forbidden transitions whose intensities show a strong angular dependence appear for $6500 < H < 7100$ G. The origin of these lines will be defined in Sec. III.

A careful examination of the experimental angular variations of the eight different sites shows that they can be approximately deduced from the angular variation of one site taken as origin by rotations in the $(\vec{z}, \vec{v})$ plane of $0.5° \pm 0.5°$, $5.0° \pm 0.5°$, $5.5° \pm 0.5°$, $6.0° \pm 0.5°$, $6.5° \pm 0.5°$, $11.0° \pm 0.5°$, and $11.5° \pm 0.5°$ (the approximations needed for this description of the eight sites will be studied in greater detail in the following sections).

Figure 5 shows a spectrum giving very clearly the eight absorption lines corresponding to the different sites for Gd^{3+}.

Figure 6 represents the angular dependence when $\vec{H}$ is rotated in the plane $(\vec{u}, \vec{z})$. In this case as well, the spectra are complicated by the existence of eight different sites.

Several angular variations were performed with the spectrometer operating in the X band. Given

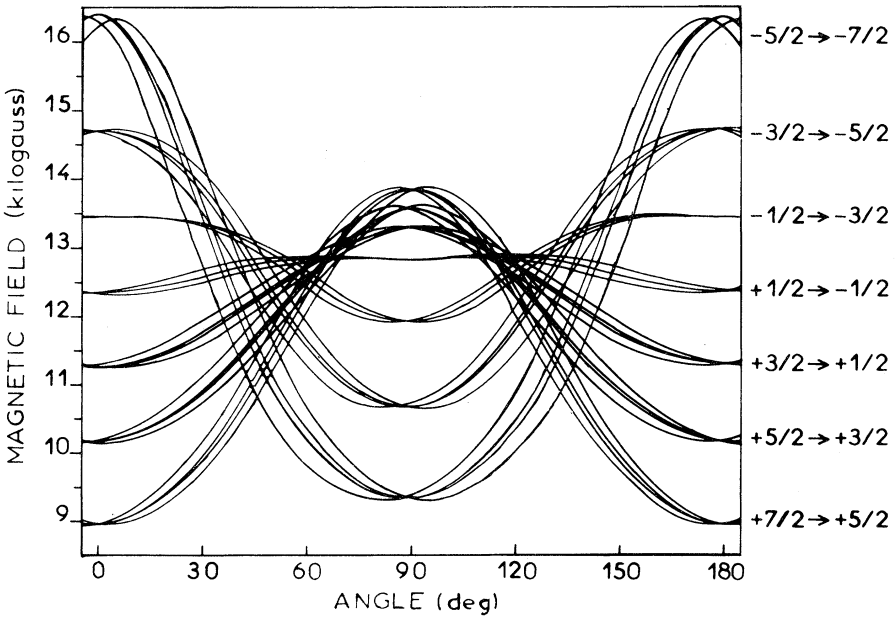

FIG. 4. Angular variations of the authorized absorption lines for Gd^{3+} in (Gd, Eu)UP. $\vec{H}$ is rotated in the plane $(\vec{u}, \vec{z})$, $\theta = 0°$ corresponds to $\vec{H} \| \vec{z}$.

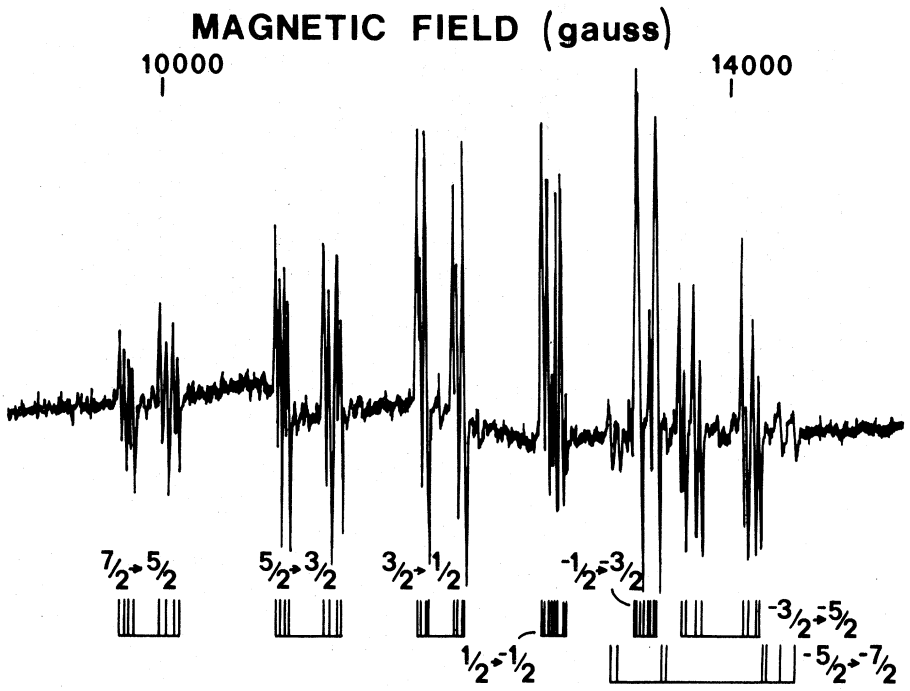

FIG. 5. EPR spectrum of (Gd, Eu)UP showing clearly the existence of eight different sites equally populated. $\vec{H}$ is in the $(\vec{u}, \vec{z})$ plane at +30° from the $\vec{z}$ axis.

the complexity of these angular variations, they will be represented and interpreted in Sec. III from the theoretical angular variations computed from the coefficients of the spin Hamiltonian obtained from the experiments in the *Ka* band.

The hyperfine structure due to odd isotopes was not observed in our experiments. This fact was probably due to the smallness of the hyperfine constants ($A \sim 5\times 10^{-4}$ cm^{-1} for Gd^{3+}) and to the width of the absorption lines (5 to 10 G for mixed UP). Of course, the relatively small number of Gd^{3+} ions inserted in mixed UP could also prevent any observation of the hyperfine and quadrupole lines of odd isotopes.

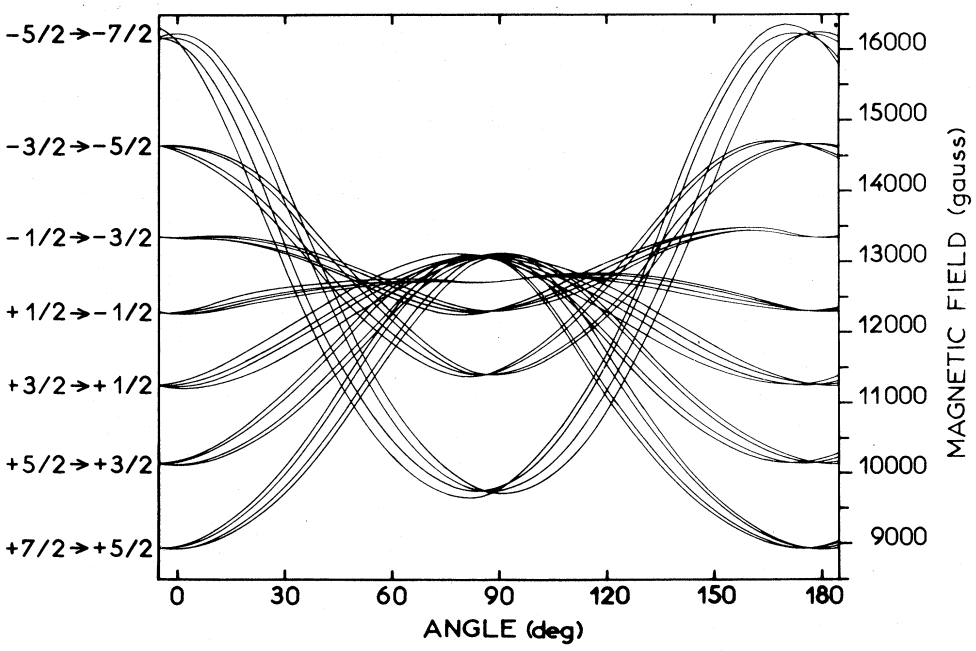

FIG. 6. Angular variations of the authorized absorption lines for (Gd, Eu)UP. $\vec{H}$ is rotated in the $(\vec{v}, \vec{z})$ plane. $\theta = 0°$ corresponds to the $\vec{z}$ axis.

III. SPIN HAMILTONIAN

A. Determination of the crystal-field parameters

The main problem was to find simultaneously the local symmetry and an axis system which would permit us to determine the independent crystal-field parameters. A program corresponding to the case of point groups C_2 or C_S was elaborated for this purpose, including point groups corresponding to higher symmetry.

Having shown in Sec. II that the hyperfine and quadrupole interactions as well as a hypothetical superhyperfine interaction due to the presence of phosphorus ions are not observed experimentally, they can be dropped from the spin Hamiltonian. This Hamiltonian is reduced to the Zeeman term $\mathcal{H}_Z$ and to the contribution $\mathcal{H}_C$ of the internal crystal field. $\mathcal{H}_Z$ and $\mathcal{H}_C$ can be written

$$\mathcal{H}_Z = \mu_B \sum_i H_i g_i S_i \ ,$$

$$\mathcal{H}_C = \sum_{k_{\text{even}}{}^{\leq 4}} B_k^q O_q^{(k)} \ ,$$

the tensor operators $O^{(k)}$ being those defined by Smith and Thornley.[20] For a ^8S-state ion and a symmetry C_2 or C_S, there are 15 independent coefficients B_k^q intervening in $\mathcal{H}_C$ and three independent components for the g tensor intervening in $\mathcal{H}_Z$ (higher-order terms in $\vec{H}$ and $\vec{S}$ will be neglected).

The determination of the B_k^q's was performed in three steps. First, $\mathcal{H}_C$ was expressed in an axis system deduced from a convenient initial axis system $\vec{x}$, $\vec{y}$, $\vec{z}$ (for example, in our case $\vec{z}$ was chosen perpendicular to the mirror plane $\vec{x}$, $\vec{y}$) by a rotation $\mathcal{R}(\alpha, \beta, \gamma)$; α, β, γ being the Euler's angles defined by Whittaker.[19] We used the relation

$$\mathcal{R}(\alpha, \beta, \gamma) O_q^{(k)} = \sum_{q'=-k}^{+k} O_{q'}^{(k)} D_{q'q}^{(k)}(\alpha, \beta, \gamma) \ ,$$

with

$$D_{q'q}^{(k)}(\alpha, \beta, \gamma) = e^{-i(\alpha q' + \gamma q)} d_{q'q}^{(k)}(\beta) \ ,$$

the $d_{q'q}^{(k)}(\beta)$ being the Wigner coefficients.[19] The $D_{q'q}^{(k)}(0, \beta, \gamma)$'s were computed for each needed value of β and γ corresponding to the chosen angular variation.

Then, the matrix elements of $\mathcal{H}_C$ were computed for each choice of β and γ from the formula[20]

$$\langle SM_S | O_q^{(k)} | SM_{S'} \rangle = \frac{1}{2^k} \left[\frac{(2S+k+1)!}{(2S-k)!} \right]^{1/2} \times (-1)^{S-M_S} \begin{pmatrix} S & k & S \\ -M_S & q & M_{S'} \end{pmatrix} .$$

The third step was to calculate the 15 independent coefficients using a least-squares-fit method by comparing the experimental position of the absorption lines with those calculated by a second-order perturbation method.

The B_k^q's were computed by minimizing the quantity

$$\sum_{i=1}^{N} X_i [\Delta W(B_k^q + \Delta B_{k_i}^q, \xi) - \Delta W(B_k^q, \xi)] = \Delta W(B_k^q, \xi) - \Delta W_{\text{expt}}(\xi) \ ,$$

where i runs over the N B_k^q's corresponding to the chosen point group. ξ represents the set of parameters M_S, β and/or γ. $\Delta W(B_k^q, \xi)$ is the energy difference between the levels M_S and $M_S - 1$, calculated from an arbitrary set of parameters B_k^q. $\Delta W(B_k^q + \Delta B_{ki}^q, \xi)$ is the value of the difference in energy of the levels M_S and $M_S - 1$ for the orientation $\alpha = 0, \beta, \gamma$ when only the ith B_k^q is increased by ΔB_{ki}^q, the others B_k^q being unchanged. $\Delta W_{\text{expt}}(\xi)$ is the experimental energy difference between the levels M_S and $M_S - 1$ for a given ξ. For example, in our case, the energy differences corresponding to the seven lines $\Delta M_S = 1$ were given for 18 values of γ, thus giving a system of 126 equations for 15 unknowns which was resolved by a least-mean-squares method.

In the last part of the calculation, the energy levels were computed by diagonalizing the 8×8 complex matrices corresponding to the calculated B_k^q's and to the chosen β and γ angles. It gives a check of the perturbation procedure and also a complete description of the energy levels in terms of the applied magnetic field, thus permitting the calculation of the positions of all authorized and forbidden absorption lines for any value of the frequency used in the experiments.[21] The program used permitted drawing automatically the angular variations of all absorption lines.

The B_k^q's were computed from the angular variation given in Fig. 3, (dashed curves) corresponding to $\alpha = 0$, $\beta = 90°$ and γ varying from 0 to 180° (γ is identical to the angle θ used in Fig. 3). The B_k^q's are given in Table I and correspond to the axis system $\vec{x}$, $\vec{y}$, $\vec{z}$ given in Fig. 1(a). These values permit fitting the experimental angular variation with an error less than 100 G. We believe that this error is due to the imprecision of the orientation of each site with respect to the growing planes taken as reference.

B. Comparison with experiments

The energy levels are given in terms of the magnetic field, for $\vec{H}$ in the $(\vec{x}, \vec{y})$ plane at 60° from the $\vec{x}$ axis in Fig. 7. The computed positions of the absorption lines for the frequencies of 35.55 and 9.2 GHz are compared to the experimental positions on the bottom of Fig. 7. The computed zero-field splitting is also given in this figure.

The computed values of the B_k^q's describe correctly the angular variations given in Figs. 4 and

TABLE I. Values of the coefficients B_k^q computed from the angular variation given in Fig. 3. These values give the angular variation of each of the eight different sites of Gd^{3+} with an error inferior to 100 G, but, of course by taking into account the rotations defined in Sec. III C, and the mirror symmetry. $\mathcal{R}$ and $\mathcal{I}$ mean real and imaginary part of the B_k^q's. $T = 300$ K; $g_x = g_y = g_z = 1.995 \pm 0.005$. The B_k^q's are given in units of 10^{-4} cm^{-1}. Neglecting the small sixth-order terms does not change very significantly the fitting to the experimental angular variations. More precisely, the standard deviation calculated with 126 experimental lines and 126 theoretical lines corresponding to Fig. 3, is 52 G when the B_q^6's are used and 64 G when the B_q^6's are neglected.

$B_0^2 = +374.1$	$B_0^6 = +0.003$
$\mathcal{R}(B_2^2) = +318.2$	$\mathcal{R}(B_2^6) = -0.006$
$\mathcal{I}(B_2^2) = -30.0$	$\mathcal{I}(B_2^6) = -0.006$
$B_0^4 = +0.384$	$\mathcal{R}(B_4^6) = +0.003$
$\mathcal{R}(B_2^4) = +0.974$	$\mathcal{I}(B_4^6) = -0.004$
$\mathcal{I}(B_2^4) = -0.409$	$\mathcal{R}(B_6^6) = +0.008$
$\mathcal{R}(B_4^4) = +0.574$	$\mathcal{I}(B_6^6) = -0.004$
$\mathcal{I}(B_4^4) = -0.784$	

6 provided that the rotations which permit passing from one site to another are taken into account.

Figure 8 represents the positions of the forbidden transition lines for $\vec{H}$ rotating in the plane $(\vec{x}, \vec{y})$ and for a frequency of 35.55 GHz. The graph is limited to $5000 < H < 12\,000$ G, corresponding to a region where the forbidden transition lines were experimentally observed. The rapid variations of the line intensities when $\vec{H}$ is rotated forbid a complete experimental description of these lines.

The computed and experimental positions of the lines appearing for $0 < \vec{H} < 7000$ G and for a frequency of 9.2 GHz are given in Fig. 9, $\vec{H}$ is rotated in the $(\vec{x}, \vec{y})$ plane. This figure gives an idea of the complexity of the spectra when low-energy photons are used. For certain orientations, 26 lines for each site exist theoretically. The lines given in Fig. 9 correspond to $\Delta M_S = 1, 2, 3$. Of course, the experimental spectra are complicated by the existence of eight different sites for Gd^{3+} (Fig. 10).

The agreement between the experimental and theoretical results for both frequencies indicates that the risk of misinterpreting the spectra is avoided.

IV. CORRELATION BETWEEN THE CRYSTAL STRUCTURE OF EuUP, GdUP, (Gd, Eu) UP AND THE MAGNETIC PROPERTIES FOR (Gd, Eu) UP

A. Crystal structure

The dimensions of the EuUP crystal used in the crystallographic study are of the order of $0.2 \times 0.15 \times 0.3$ mm^3.

Data were collected at room temperature on a Sintex $P2_1$ four circles diffractometer using 2θ scanning with filtered Mo $K\alpha$ radiation. We found the parameters of the monoclinic unit cell ($Z = 4$) to be $a = (8.744 \pm 0.001)$ Å, $b = (12.949 \pm 0.002)$ Å,

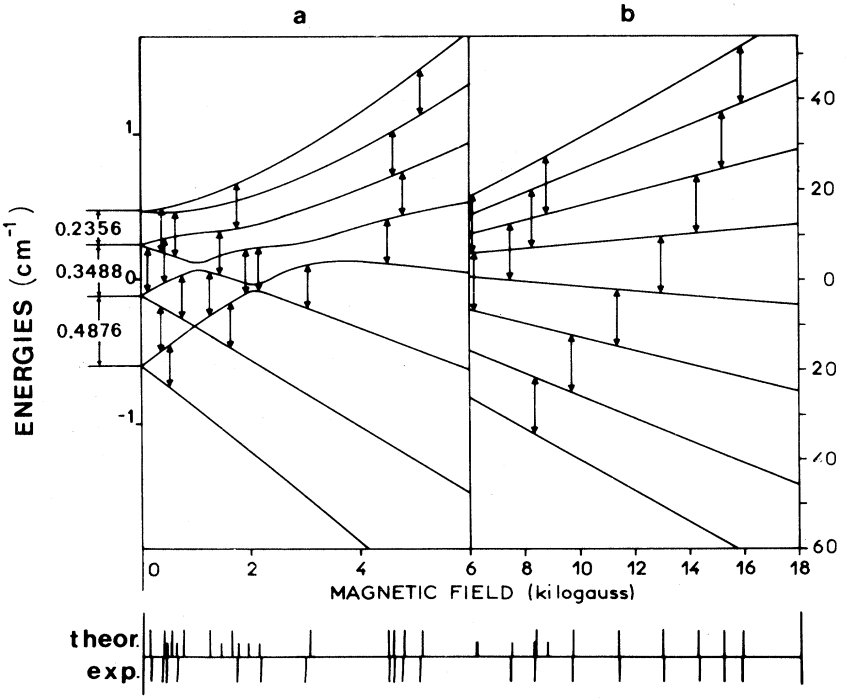

FIG. 7. Representation of the energy levels in terms of H. $\vec{H}$ is in the plane $(\vec{x}, \vec{y})$ at 60° from the $\vec{x}$ axis; (a) gives the energy levels and all authorized and forbidden absorption lines. Frequency 9.2 GHz. The zero-field splitting is also given in this figure; (b) gives the positions of the absorption lines for a frequency of 35.55 GHz.

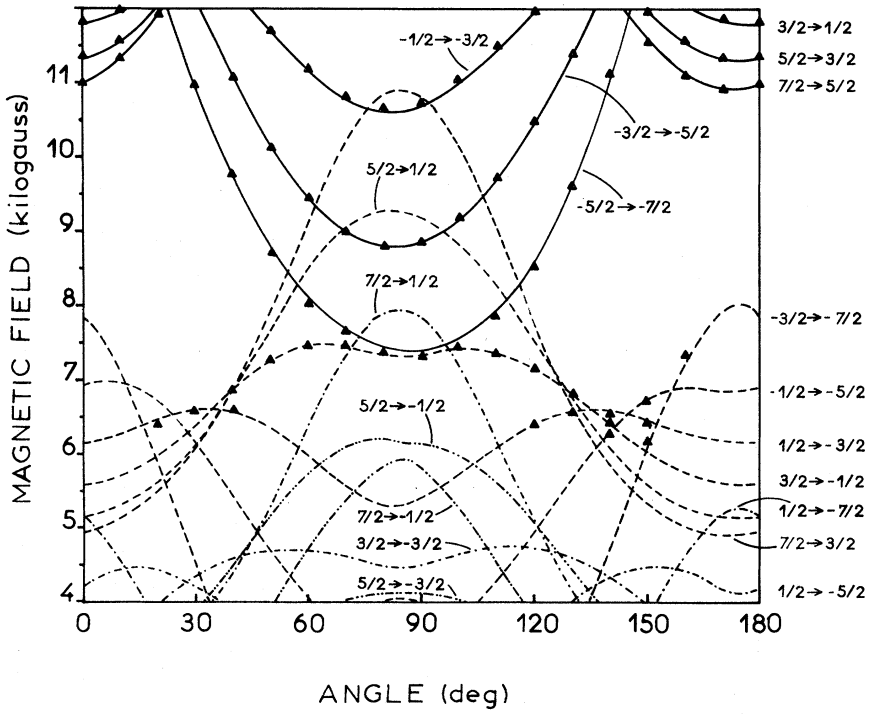

FIG. 8. (Gd, Eu)UP. *Ka* band. Forbidden transitions (dashed curves) appearing for $5000 < H < 11\,000$ G. $\vec{H}$ is rotated in the $(\vec{x}, \vec{y})$ plane. Only half of the absorption lines corresponding to the eight sites are represented in this figure. The others are obtained by performing a mirror symmetry at $\theta = 45°$. The authorized transition lines are represented by the solid curves.

$c = (8.925 \pm 0.002)$ Å, $\gamma = 90.46° \pm 0.02°$.

The systematic absences *hko* with $k = 2n+1$ and *ool* with $l = 2n+1$ are consistent with the space group $P2_{1/b}$. The intensities of all 3271 independent reflections were measured between $2\theta = 0°$ and $2\theta = 65°$. No reflection was suppressed. Reflections with negative intensities were set to zero and were retained for the refinement. Corrections were made for sample absorption, Lorentz and polarization factors.

A straightforward interpretation of the three-dimensional Patterson synthesis of the $|F|^2$ data placed the europium atoms in fourfold special positions $4(l)$ of $P2_{1/b}$. Refinement cycles and successive difference Fourier syntheses ($F_{obs} - F_{calc}$) allowed us to locate the positions of 20 phosphorous and 56 oxygen atoms without any chemical assumption. No other atoms were observed because no peak of electronic density was higher than three electrons. The discrepancy factor obtained at this stage was $R = 0.061$. However, for the strong reflections near the origin of the reciprocal lattice, the differences $F_{obs} - F_{calc}$ were systematically negative. Furthermore, during the B and K calculation by the Wilson method, we observed that for the small values of $\langle \sin^2\theta/\lambda^2 \rangle$ the $\langle |E| \rangle^2$ values were below the unity, indicating a strong secondary extinction. At this stage, a refinement on the secondary isotropic extinction coefficient (there is only one coefficient, all the reflections being in the same scale) was made by inserting the 3271 reflec-

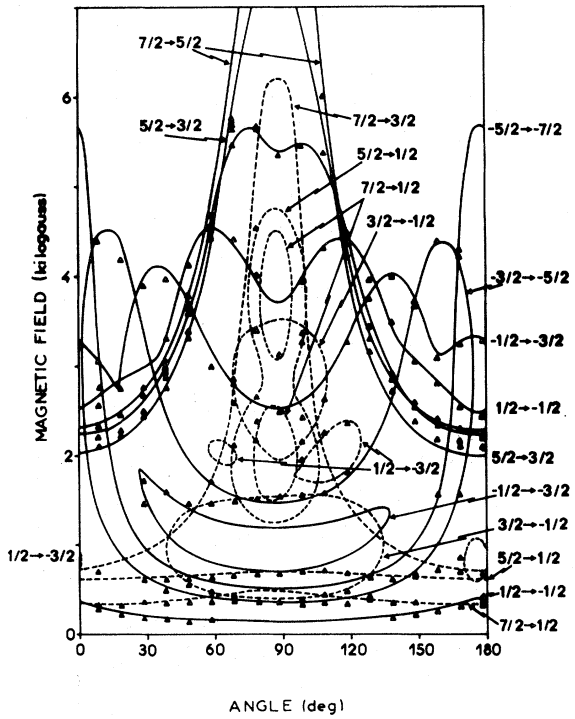

FIG. 9. (Gd, Eu)UP. Authorized and forbidden transitions obtained at 9.2 GHz. $\vec{H}$ is rotated in the $(\vec{x}, \vec{y})$ plane. This graph must be completed by the graph obtained by doing a mirror symmetry at $\theta = 45°$. Given the complexity of the experimental spectra, only unambiguously defined absorption lines are reported on this figure.

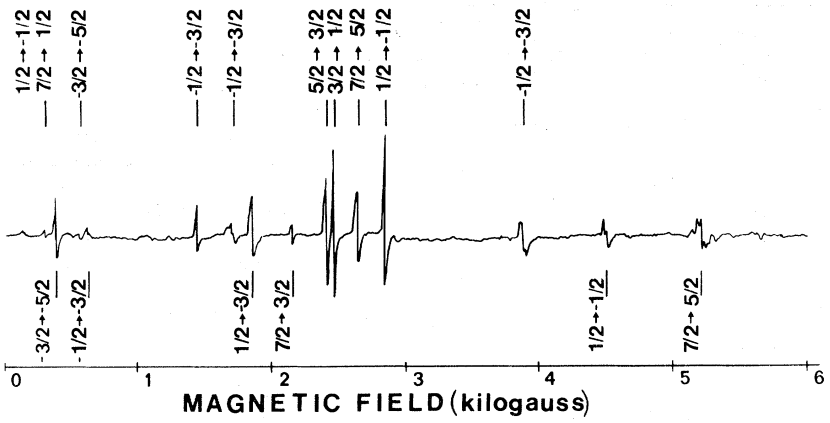

FIG. 10. (Gd, Eu)UP, X band. EPR spectrum corresponding to the angle $\theta = 70°$ in Fig. 9.

tions in the ORXFL-3 program of Busing *et al.*[22] We then obtained a final R value of 0.040. Cycles of least-squares refinement employing anisotropic temperature factors for europium atoms showed an insignificant anisotropy. We therefore kept the isotropic factors (Table II).

The oxygen atoms around a europium atom form an eight-coordinate polyhedron [Fig. 1(b)] with a mean distance Eu-O of 2.411 Å (Table III). The phosphorous atoms are located in tetrahedra with a mean distance P-O of 1.538 Å(Table IV). The bond angles O-P-O are listed in Table V. In a unit cell, four $(PO_4)^{3-}$ chains, zigzagging up the a axis are constituted by the sequences P_1-P_4-P_5-P_2-P_1, etc. Each tetrahedron $(PO_4)^{3-}$ is joined at an apex with two neighboring tetrahedra in the chain. Furthermore, loops P_2-P_3-P_4 connect the chains by tetrahedra sharing corners. Each of the eight oxygen atoms bonded to Eu is given by a different tetrahedron. So the rare earth is surrounded by eight $(PO_4)^{3-}$ tetrahedra (two tetrahedra for each independent phosphorous atom). Each P_1, P_5, and P_3 phosphorous atom possesses two P-O-P bonds with two other phosphorous atoms and two P-O-Eu bonds with two europium atoms. On the other hand, the P_4 and P_2 phosphorous atoms possess three P-O-P bonds and only one P-O-Eu bond (Figs. 11 and 12).

Two important results for the EPR study can be deduced from the above structure determination of EuP_5O_{14}. First, the point symmetry for europium is C_S. Second, europium is placed in fourfold general positions $4(l)$:

$$x, y, z;\ \bar{x}, \bar{y}, \bar{z};\ \bar{x}, \tfrac{1}{2}-y, \tfrac{1}{2}+z;\ x, \tfrac{1}{2}+y, \tfrac{1}{2}-z\ .$$

Thus, europium ions are related to each other by two pseudo mirror planes. Since the two planes containing the oxygen atoms O_{11}, O_2, O_{13} and O_5, O_1, O_{14} are not only symmetrical with respect to the pseudo mirror plane giving the C_S symmetry but secant as well, there are four differently oriented surroundings for Eu^{3+} in the crystals.

Experiments were also made on GdUP and mixed (Gd, Eu) UP. We found that GdUP and EuUP crystallize in the same monoclinic system $P2_{1/b}$, and

TABLE II. Positional parameters for EuP_5O_{14}. The B's are the individual isotropic temperature factors. The precision σ is indicated in parentheses.

Ions	X	Y	Z	B
Eu	0.27728 (3)	0.49887 (2)	0.80965 (2)	0.63 (1)
P_1	0.0062 (2)	0.1725 (1)	0.5023 (2)	0.62 (2)
P_2	0.2447 (2)	0.3347 (1)	0.4526 (2)	0.66 (2)
P_3	0.3147 (1)	0.4999 (1)	0.2451 (2)	0.62 (2)
P_4	0.2275 (2)	0.6640 (1)	0.4489 (2)	0.63 (2)
P_5	0.4924 (2)	0.7971 (1)	0.4950 (2)	0.68 (2)
O_1	−0.0834 (5)	0.1215 (3)	0.3843 (5)	1.28 (6)
O_2	0.0793 (5)	0.1135 (3)	0.6238 (5)	1.24 (6)
O_3	0.1336 (5)	0.2440 (3)	0.4199 (5)	1.27 (6)
O_4	−0.0918 (5)	0.2617 (3)	0.5831 (5)	1.28 (6)
O_5	0.2209 (5)	0.3895 (4)	0.5937 (5)	1.46 (7)
O_6	0.2213 (5)	0.4012 (3)	0.3089 (5)	1.19 (6)
O_7	0.5926 (5)	0.7099 (4)	0.5735 (5)	1.41 (7)
O_8	0.2908 (5)	0.5003 (3)	0.0813 (5)	1.39 (7)
O_9	0.4683 (5)	0.5048 (3)	0.3130 (5)	1.14 (6)
O_{10}	0.2064 (5)	0.5889 (3)	0.3140 (5)	1.21 (6)
O_{11}	0.2320 (5)	0.6154 (4)	0.5955 (5)	1.63 (7)
O_{12}	0.3729 (5)	0.7263 (3)	0.4027 (5)	1.37 (7)
O_{13}	0.4115 (5)	0.8503 (3)	0.6158 (5)	1.31 (6)
O_{14}	0.5853 (5)	0.8517 (3)	0.3818 (5)	1.23 (6)

TABLE III. Bond distances Eu-O. σ is given in parentheses.

Bond	Length (Å)
Eu-O_{13}	2.357 (5)
Eu-O_{14}	2.359 (7)
Eu-O_2	2.365 (7)
Eu-O_1	2.388 (5)
Eu-O_8	2.428 (8)
Eu-O_5	2.440 (5)
Eu-O_{11}	2.469 (7)
Eu-O_9	2.480 (7)

TABLE IV. Bond distances P-O. σ is given in parentheses.

Bond	Length (Å)
P_1O_1	1.467 (7)
P_1O_2	1.475 (10)
P_1O_4	1.614 (8)
P_1O_3	1.619 (7)
P_2O_5	1.461 (8)
P_2O_3	1.547 (10)
P_2O_7	1.557 (7)
P_2O_6	1.560 (7)
P_3O_9	1.474 (8)
P_3O_8	1.477 (8)
P_3O_6	1.614 (7)
P_3O_{10}	1.619 (7)
P_4O_{11}	1.453 (10)
P_4O_{12}	1.556 (8)
P_4O_{10}	1.558 (8)
P_4O_4	1.560 (7)
P_5O_{13}	1.465 (7)
P_5O_{14}	1.473 (8)
P_5O_7	1.596 (8)
P_5O_{12}	1.611 (10)

therefore, the Eu^{3+} (ionic radius = 1.03 Å for coordination number 6) substitution by Gd^{3+} (ionic radius = 1.02 Å) involves no change in lattice cohesion. On the other hand, mixed (Gd_xEu_{1-x}) UP with $x = 5\times10^{-2}$ at.% presented the same crystallographic structure as pure EuUP.

TABLE V. Bond angles O-P-O in degrees. σ is given in parentheses.

$O_1P_1O_2$	121.8 (1)
$O_1P_1O_4$	111.0 (1)
$O_1P_1O_3$	107.1 (1)
$O_2P_1O_4$	106.0 (1)
$O_2P_1O_3$	109.4 (1)
$O_4P_1O_3$	99.2 (1)
$O_5P_2O_3$	116.1 (1)
$O_5P_2O_7$	116.3 (1)
$O_5P_2O_6$	114.9 (1)
$O_3P_2O_7$	105.1 (1)
$O_3P_2O_6$	100.4 (1)
$O_7P_2O_6$	101.9 (1)
$O_9P_3O_8$	122.4 (1)
$O_9P_3O_6$	110.1 (1)
$O_9P_3O_{10}$	110.5 (1)
$O_8P_3O_6$	106.3 (1)
$O_8P_3O_{10}$	106.8 (1)
$O_6P_3O_{10}$	97.7 (1)
$O_{11}P_4O_{12}$	116.0 (1)
$O_{11}P_4O_{10}$	115.4 (1)
$O_{11}P_4O_4$	117.1 (1)
$O_{12}P_4O_{10}$	102.2 (1)
$O_{12}P_4O_4$	104.7 (1)
$O_{10}P_4O_4$	99.0 (1)
$O_{13}P_5O_{14}$	123.0 (1)
$O_{13}P_5O_7$	106.2 (1)
$O_{13}P_5O_{12}$	109.3 (1)
$O_{14}P_5O_7$	109.7 (1)
$O_{14}P_5O_{12}$	105.9 (1)
$O_7P_5O_{12}$	100.3 (1)

At this time, our results can be compared only to those of Bagieu-Beucher, and we are in agreement (for both GdUP and EuUP the space group is $P_{21/a}$). Since we did not observe twinnings in EuUP, hypothesis (ii) (Sec. I) of Albrand *et al.* could explain the contradictory structures obtained for NdP_5O_{14}.

B. Magnetic results

The most detailed result obtained by EPR experiments concerning the mixed UP's was the determination of the presence of eight different sites for Gd^{3+} introduced as impurity in EuUP.

These different sites appeared in all studied crystals. Complementary experiments performed both by EPR and x-ray techniques on very small

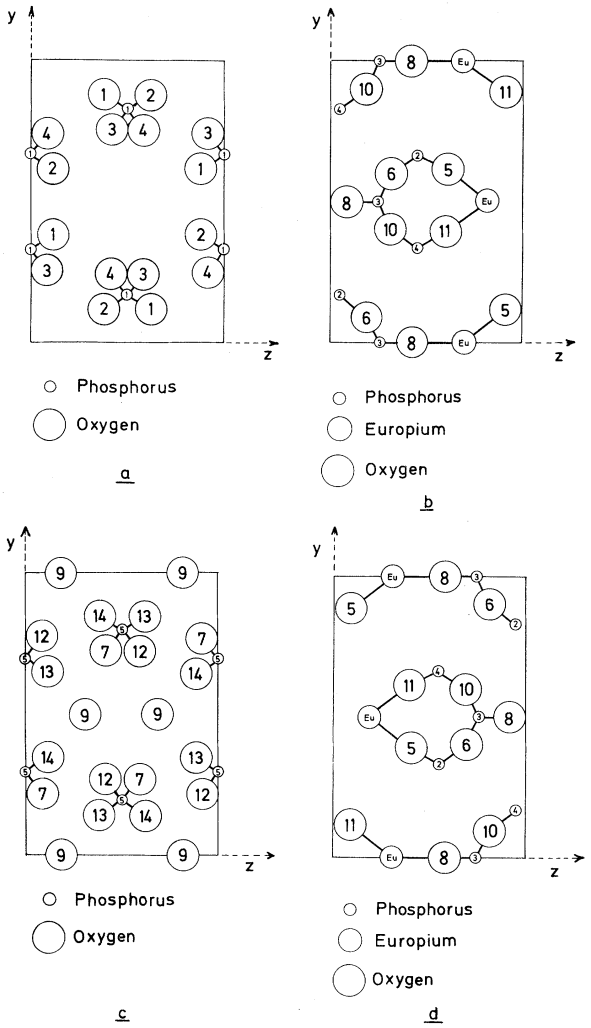

FIG. 11. Projections on the planes Oyz (a), $\frac{1}{4}yz$ (b), $\frac{1}{2}yz$ (c), and $\frac{3}{4}yz$ (d) of the nearest ions of these different planes.

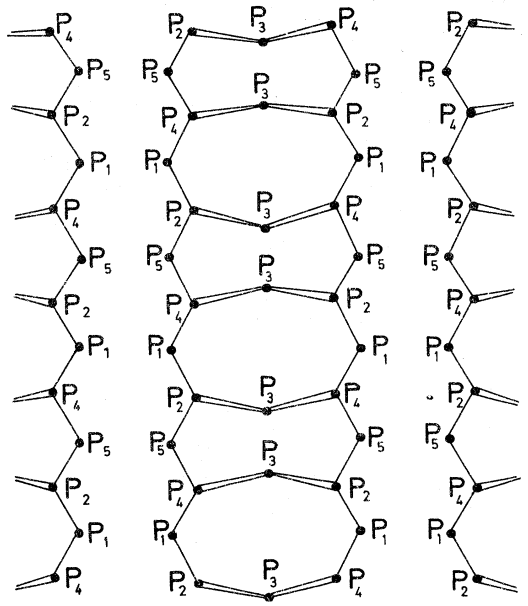

FIG. 12. Projection of the ultraphosphate structure on the $(\vec{x},\vec{y})$ plane showing the chains of PO_4 tetrahedra sharing tops.

Gd_xEu_{1-x} crystals with dimensions of the order of $0.1\times0.1\times0.1$ mm^3 (and $x=0.1$ at.% in order to get an acceptable signal-to-noise ratio in EPR experiments) showed the presence of eight Gd^{3+} sites, but the crystal structure found by x-ray experiments was identical to that of pure EuUP$_5$.

The relative orientations of the eight Gd^{3+} sites compatible with angular variations of Figs. 3, 4, and 6 have been determined, the scheme is given in Fig. 13, in the reference axis system taken in Fig. 1. Thus, the introduction of Gd^{3+} ions in EuUP distorts slightly the lattice but the symmetry properties of the Gd^{3+} sites determined by EPR remain identical to those of Eu^{3+} sites determined by x-ray experiments.

More precisely, the results obtained from EPR experiments permit concluding first, that the point symmetry of Gd^{3+} sites in EuUP is C_S. This is the pseudo point symmetry determined by x-ray measurements for Eu^{3+} in EuUP and (Gd, Eu) UP.

On the other hand, an interesting problem was to give an interpretation of the mirror angular variations appearing in Fig. 3. The most simple interpretation rested on the existence of at least one mirror plane between two Gd^{3+} ions. The possible mirror planes being either the $(\vec{u},\vec{z})$ plane or the $(\vec{v},\vec{z})$ plane or both simultaneously. X-ray measurements confirmed the presence of two pseudo mirror planes $(\vec{u},\vec{z})$ and $(\vec{v},\vec{z})$ between different Eu^{3+} ions in EuUP and (Gd, Eu) UP. Thus, the Gd^{3+} ions appear to be related by the same symmetry relations as the Eu^{3+} ions.

We have not attempted to give a detailed interpretation of the linewidths for GdUP. We will only emphasize the fact that crystallographic studies give the same structure for GdUP and for EuUP, so that the results obtained for (Gd, Eu) UP can be considered as a good start for studies of this kind. Of course, not only Gd-Gd magnetic interactions should be taken into account but also the existence of eight and perhaps more different sites which could not be separated by x-ray studies and which could also contribute to the linewidths.

V. CONCLUSION

The spin Hamiltonian of Gd^{3+} ions in EuUP has been determined completely. Moreover, the EPR experiments have shown that eight Gd^{3+} centers appear in (Gd, Eu) UP. It has been demonstrated that these centers result from slight distortions of the EuUP lattice due to the presence of Gd^{3+} ions but that the point symmetry for Gd^{3+} sites and the symmetry relations between different Gd^{3+} ions are in agreement with those determined for Eu^{3+} in pure and mixed UP. In addition, the first complete structure analysis with all interatomic distances and bond angles has been given for EuUP.

ACKNOWLEDGMENTS

We wish to thank Dr. J. P. Denis for his participation in the crystal growing. One of us (R. P.) would like to thank Dr. S. A. Marshall for very fruitful discussions. We appreciate the deep interest shown in this work by Dr. J. Loriers, Professor D. Curie and Professor J. Mattler.

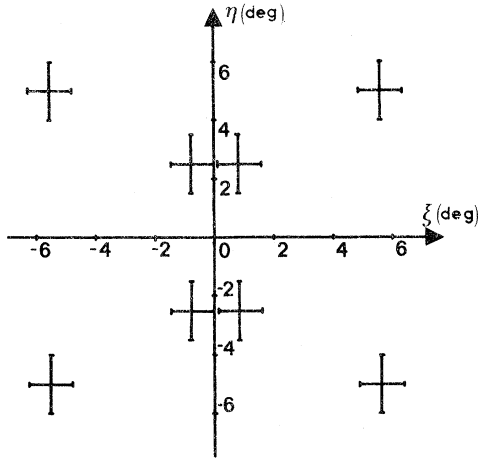

FIG. 13. Representation of the approximate orientation of the z axes of the different sites for Gd^{3+} in (Eu, Gd)UP. ξ is the angle between the z axis defined in Fig. 1 with respect to the crystal and the projection on the $(\vec{u},\vec{z})$ plane of the $\vec{z}$ axis of the site. η is the angle between the $\vec{z}$ axis defined in Fig. 1(a) and the projection on the $(\vec{v},\vec{z})$ plane of the $\vec{z}$ axis of the site. Each cross formed by the error bars gives the approximate position of two different sites which cannot be distinguished very precisely from each other.

[1]An analysis of many mechanisms contributing to the ground-state splitting of gadolinium has been given by B. G. Wybourne, Phys. Rev. 148, 317 (1966).
[2]M. M. Abraham, L. A. Boatner, Y. Chen, J. L. Kolopus, and R. W. Reynolds, Phys. Rev. B 4, 2853 (1971).
[3]M. M. Abraham, C. B. Finch, J. L. Kolopus, and J. T. Lewis, Phys. Rev. B 3, 2855 (1971).
[4]G. Bacquet, J. Dugas, C. Escribe, L. Vassiliev, and B. M. Wanklyn, Phys. Rev. B 5, 2419 (1972).
[5]J. Rosenthal, R. F. Riley, and U. Ranon, Phys. Rev. 177, 625 (1969).
[6]J. Rosenthal, Phys. Rev. 164, 363 (1967).
[7]J. C. Danner, U. Ranon, and D. N. Stamires, Phys. Rev. B 3, 2141 (1971).
[8]C. A. Hutchison, B. R. Judd, and D. F. D. Pope, Proc. Phys. Soc. Lond. B 70, 514 (1957).
[9]B. Bleaney, R. J. Elliot, H. E. D. Scovil, and R. S. Trenam, Philos. Mag. 42, 1062 (1951).
[10]B. Bleaney, H. E. D. Scovil, and R. S. Trenam, Proc. R. Soc. Lond. A 223, 15 (1954).
[11]B. Blanzat, J. P. Denis, and J. Loriers, in Proceedings of the International Conference on Rare Earth, 1973 (U. S. AEC, Oak Ridge, Tenn., 1973).
[12]S. Jaulmes, C. R. Acad. Sci. C 268, 935 (1969).
[13]M. Bagieu-Beucher and Duc Tranqui, Bull. Soc. Fr. Mineral. Cristallogr. 93, 505 (1970).
[14]H. G. Danielmeyer and H. P. Weber, J. Quant. Elect. 8, 805 (1972).
[15]Duc Tranqui, M. Bagieu-Beucher, and A. Durif, Bull. Soc. Fr. Mineral. Cristallogr. 95, 437 (1972).
[16]H. Y. P. Hong and J. W. Pierce, Mater. Res. Bull. 9, 179 (1974).
[17]K. R. Albrand, R. Attig, J. Fenner, J. P. Jeser, and D. Mootz, Mater. Res. Bull. 9, 129 (1974).
[18]S. A. Marshall, Phys. Rev. 159, 191 (1967).
[19]H. Watanabe, *Operator Methods in Ligand Field Theory* (Prentice-Hall, Englewood Cliffs, N. J., 1966).
[20]D. Smith and J. H. M. Thornley, Proc. Phys. Soc. Lond. 89, 779 (1966).
[21]The diagonalization of the energy matrix and the comparison of the experimental and calculated angular variations of the absorption lines for two different frequencies (9.2 and 35.55 GHz in our case) permitted avoiding any erroneous determination of the zero-field splitting of Gd^{3+}. Some cases where a miscalculation of the zero-field splitting can occur, have been studied by M. I. Darby, J. Chem. Phys. 58, 2145 (1973).
[22]W. R. Busing, K. C. Martin, and H. A. Levy (private communication).